Effect of Diffusion on Heterogenous Ethylene Propylene Copolymerization

E. L. Hoel and C. Cozewith
Exxon Chemical Co., Linden, NJ 07036

G. D. Byrne
Exxon Research and Engineering Co., Annandale, NJ 08801

In heterogenous olefin polymerization with Ziegler catalysts, the influence of monomer mass transport in the growing granule on polymer properties has been extensively modeled, but it has not been possible to clearly establish the importance of diffusion experimentally since the multisited nature of most Ziegler catalysts can produce similar effects. In this study, ethylene-propylene copolymers were made with single-sited metallocene catalysts by slurry polymerization in liquid monomers. These copolymers had a relatively narrow molecular weight distribution with a composition distribution (CD) broader than expected for a single-site catalyst. Data analysis indicates that mass-transfer limitations in the polymer particles are the most likely explanation for the observed results. For amorphous copolymers, a diffusion/reaction model could predict CD breadth in good agreement with experimental data, but for semicrystalline polymers the model was inaccurate. We postulate that model inadequacies are due to radial gradients in monomer diffusivity during polymerization which the model does not account for.

Introduction

The vast majority of the billions of pounds of polyolefins produced each year by Ziegler-Natta catalysts are made in multiphase reactors where the polymer exists as granules suspended in a fluid containing the monomers. For the most part, Ziegler polyolefins have a broad molecular weight distribution (MWD) with a ratio of weight to number average molecular weight (Q) of greater than 2 (4 to 10 is typical). Early investigations recognized that likely explanations of broad MWD included multiple active catalyst sites in the catalyst and non-steady-state effects at the active site due to mass transport limitations (Zucchini and Cecchin, 1983). Initial attempts (Bul and Higgins, 1970) to model the diffusion/reaction process at an active site embedded in a matrix of polymer indicated that diffusion alone could account for the observed MWDs. However, a large body of evidence now exists (see Zucchini and Checcin, 1983; Cozewith, 1987; Yechevskaya et al., 1987; and Haejaski et al., 1988) showing that multisited Ziegler catalysts are the rule rather than the exception. Thus, diffusion may indeed have an influence on polymerization rates and polymer properties, but if so, it would be very difficult to distinguish from the complicated polymerization behavior resulting from the multiple active sites. Consequently, there is no unequivocal data published in the literature that demonstrates whether polymer phase mass transport effects are important in Ziegler polymerizations.

Recently, a new class of olefin polymerization coordination catalysts was discovered (Sinn et al., 1980) based on metallocene compounds of zirconium, titanium, or hafnium combined with an activator such as methyl alumoxane. These catalyst systems are capable of making the same range of olefin homo- and copolymers as Ziegler-Natta catalysts, however, they tend to be single-sited and to produce polymers with a most probable ($M_w/M_n = 2$) molecular weight distribution. In multiphase polymerizations with single-sited metallocene catalysts, deviations from the polymerization rate behavior or polymer properties expected for kinetically controlled reactions might well be strong evidence for diffusional effects on the polymerization.

We have studied the copolymerization of ethylene and pro-

Present address of G. D. Byrne: Dept. of Mathematics, Illinois Institute of Technology, Chicago, IL 60616.

pylene catalyzed by metallocenes combined with an activator on a silica support. Slurry polymerizations were carried out in a medium of the liquid monomers. Fractionation of the copolymer revealed a narrow MWD ($2<Q<2.5$), but a broad composition distribution. In this article, we present the polymerization rate and polymer analysis data from this study, and try to determine whether diffusional effects can account for the results. We also present a new computer algorithm for solving the equations of the polymeric flow diffusion/reaction model for polymerization in a growing granule and compare model predictions to the experimental data.

Experimental Studies

Catalyst preparation

Two different metallocenes were used as catalysts (catalysts A and B). They differed primarily in the steric arrangement of the ligands around the metal atom, with catalyst A having a more "open" active site. As a result, catalyst A incorporates propylene into the copolymer much more readily than catalyst B.

Supported catalysts were prepared by first slurrying oven dried (800°) Davison 948X silica gel in a hydrocarbon and adding a solution of the catalyst activator. All steps in catalyst preparation were carried out with purified materials under a N_2 atmosphere. The slurry was then evaporated to dryness to deposit the activator in the silica pores. The dry SiO_2/activator powder was reslurried in hydrocarbon, and a solution of the metallocene compound was added. After allowing sufficient time for the metallocene to react with the activator on the silica, ethylene was bubbled through the slurry to initiate the polymerization and form a prepolymer to begin breakup of the SiO_2 structure. Typically, the amount of PE produced was somewhat more than the amount needed to just fill the pores of the support (200-300% by weight of the catalyst prior to prepolymerization). The slurry was evaporated to dryness, and the final catalyst was recovered as a fine, free flowing powder. Metallocene concentration in the final catalyst was on the order of 10^{-5} mol/g.

Polymerization

Laboratory polymerizations were carried out in a 1 liter Zipperclave autoclave (manufactured by Autoclave Engineers) operated in the semibatch mode. Agitation was provided by a 2.54 cm diameter turbine impeller (7.0 cm reactor diameter) at 550 rpm. Prior to adding reactants, the reactor was baked at 130°C under N_2, cooled to room temperature with a N_2 flush, and treated with a small amount of triethyl aluminum (TEAL) to eliminate any trace catalyst poisons that might remain. Past experiments had indicated the quantity of TEAL needed to optimize catalyst activity. The reactor was then partially filled with liquid propylene (typically 500 cm^3), brought to temperature, and gaseous ethylene was added to raise the pressure to the desired target level. The reactor was operated at vapor-liquid equilibrium so that the liquid-phase monomer composition could be calculated from the reactor temperature and pressure. The SRK VLE correlation in the PROCESS program thermodynamic package was used for this calculation. Polymerizations were carried out at 25-60°C with pressures between 20-40 atm. At a given temperature, the comonomer concentrations in solution were varied by changing the total pressure.

After the reactor was at run conditions, catalyst was added from a pressurized injection device to start the polymerization. A pressure control system added ethylene continuously from a feed bomb to maintain reactor pressure constant as ethylene was consumed. The ethylene reaction rate could be followed by measuring the rate of pressure decrease in the bomb. Propylene was always present in large excess. Temperature was held constant by circulating coolant through the reactor jacket on automatic control. At the end of a run the pressure in the reactor was slowly reduced to atmospheric to vent the monomer, the reactor was opened and the polymer recovered, and the polymer was dried overnight in a vacuum oven for final removal of monomer.

The data discussed in this report were obtained from runs in which the reaction conditions gave polymer particle slurries in the liquid monomer during polymerization. Depending on polymer composition and molecular weight, the polymer granules could be either essentially single particles 0.5-1 mm in diameter with a narrow size distribution, or a mixture of single and agglomerated particles, of broader size distribution. To obtain polymer slurries it is important to avoid large initial exotherms on catalyst addition, high slurry concentration, and low polymer molecular weight.

Polymer analysis

Polymers were analyzed for ethylene content by FTIR, molecular weight by GPC and sequence distribution by ^{13}C NMR using techniques described earlier (Cozewith, 1987). The polymers were fractionated by adding isopropanol incrementally to a polymer solution in cyclohexane to precipitate the polymer gradually. Solutions were prepared by adding 1.25 g of polymer, cut into small pieces, to 250 cm^3 of cyclohexane and stirring the mixture gently for at least 24 h at room temperature. The solution was then poured through a tared, 100 mesh stainless steel screen to remove insoluble polymer. This polymer fraction was then dried, weighed, and analyzed for ethylene content. This is the first fraction. The identical filtration and drying procedure is used for all successive fractions.

After removal of insoluble polymer, isopropanol is slowly titrated into the solution until polymer starts to precipitate. We attempt to add an amount that precipitates about 0.1-0.2 g of polymer, and this is judged visually. The precipitated polymer is removed as described above, and more alcohol is added to precipitate another fraction. The process is continued until 6-8 fractions are obtained. Then the solution is evaporated to dryness to recover the remaining soluble polymer as the final polymer fraction. We have found that fractions first precipitate in order of decreasing crystallinity, and then, when the amorphous composition range (<55 wt. % ethylene) is reached, in order of descending molecular weight.

Copolymer Composition Distribution

The conditions in our polymerizations were designed to give a constant comonomer ratio during chain growth. Copolymerization with a single-sited catalyst under these conditions should result in a very narrow copolymer composition distribution (CD) (Stockmeyer, 1945). In fact, ethylene-propylene copolymer made in solution polymerization with single-sited

Table 1. Polymerization Conditions for Fractionated Samples

Figure	Catalyst	Temp. °C	Poly Time Min	$M_{10} \times 10^3$ mol/cm^3	M_{10}/M_{20}	Copoly. Comp. wt. %C_2=
1	A	50	30	1.42	0.408	59.0
	B	55	60	0.511	0.096	58.5
5	B	50	20	0.684	0.141	74.9
	B	50	40	0.684	0.141	70.5
	B	50	60	0.684	0.141	64.4
15	A	40	27	1.16	0.314	55.1
19	B	50	60	0.684	0.141	64.4
22	B	35	57	0.594	0.127	63.6
	B	50	60	0.684	0.141	64.4
23	A	30	30	1.60	0.602	58.8
	A	40	27	1.16	0.314	55.1
	A	50	30	1.42	0.408	59.0

vanadium catalyst fractionated by the technique described in the experimental section typically gives fractions with ethylene contents differing no more than ±1 wt. % ethylene from the mean value.

Fractionation of copolymer samples A1 and B1 made in slurry polymerization with catalysts A and B at the conditions shown in Table 1 gave the cumulative composition distributions shown in Figure 1. The CD data presented in this and all following cumulative distribution plots have the composition of the first fraction to precipitate appearing on the left of the X-axis. The polymer made with B catalyst has a remarkably broad composition distribution.Polymer species are present that range from 43.8 to 72.2 wt. % ethylene: a spread of 28.4 wt. %. On the other hand, the polymer of the same average composition made with A catalyst has a much narrower CD. The compositional spread is 7.2 wt. % and about 85% of the copolymer is within ±2% of the mean composition. However, even in this case, the CD is much broader than expected for polymerization with single-site catalysts at constant comonomer concentration. On the other hand, the M_w/M_n values of 2.3 and 2.6 for A and B catalyst polymers, respectively, are indicative of Ziegler polymerization with predominantly one catalyst species.

The CD breadths illustrated in Figure 1 are characteristic of the products made with these two catalysts over a broad range of polymerization conditions, as will be shown by additional CD data discussed later. Narrow MWD with M_w/M_n generally between 2-2.5 is also a polymer characteristic.

A series of runs made with B catalyst at 50°C and a liquid-phase monomer ratio of 0.14 mol C_2=/mol C_3= but with polymerization time varying from 2 to 60 min indicated that average copolymer ethylene content decreased with time, as shown by the results in Figure 2. Polymer composition was independent of time in polymerizations with A catalyst. The molecular weight of the polymers in Figure 2 decreased with time; however, MWD remained constant as indicated by a narrow range of Q values (see Figure 3). The molecular weight decrease is probably related to the polymer composition since, with both A and B catalysts, we found that M_n generally falls as comonomer content is raised, presumably due to chain transfer reactions involving propylene ended chains. Despite the variations in ethylene content with time, Figure 4 shows that polymer yield was directly proportional to polymerization time for these runs, indicating that polymerization rate was con-

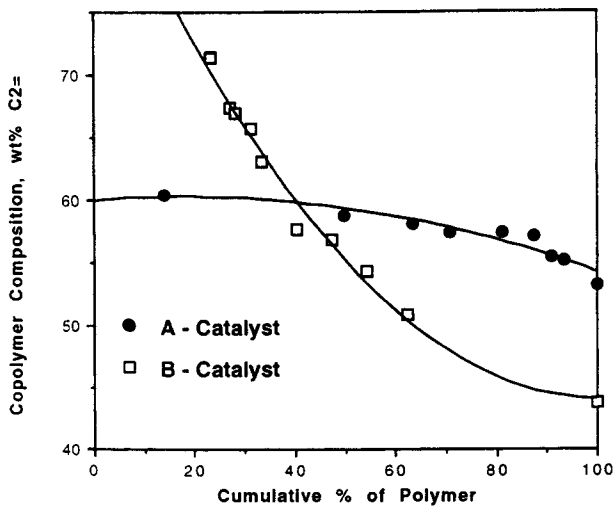

Figure 1. Composition distribution for A and B catalyst copolymers.

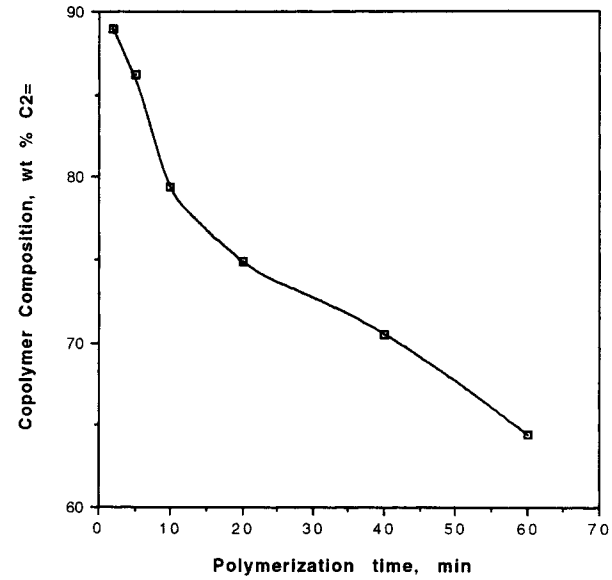

Figure 2. Variation of copolymer composition with time in B catalyst polymerization.

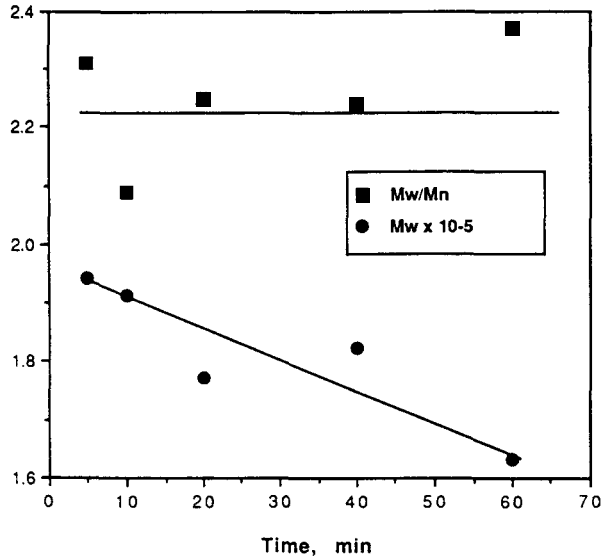

Figure 3. Variation of polymer MW and MWD with time in B catalyst polymerization.

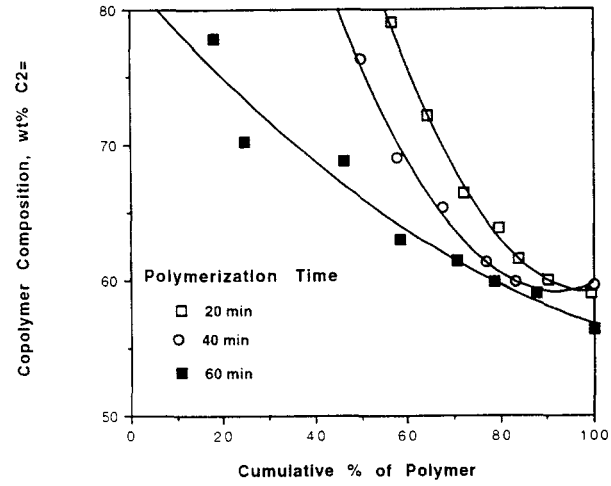

Figure 5. Change of polymer CD with time in B catalyst polymerization.

stant. Measurements of polymerization rates with both A and B catalysts over a broad range of conditions indicates that constant reaction rate, at least up to times of 60 min, is a general characteristic of these catalysts. Composition distribution determinations (see Figure 5) for the B catalyst copolymers made at 20, 40 and 60 min polymerization time shows a broadening of the CD as time increases due to an increase in the amount of low ethylene content polymer. This result is, of course, consistent with the time variation of average composition shown in Figure 2.

To further characterize the B catalyst polymers, a 175-micron particle made at 5 min reaction time was sectioned by low-temperature microtoming so that the internal structure could be examined. Figure 6 shows a surface layer of polymer is present, about 10-micron-thick, that appears to have a different morphology than the polymer in the granule interior.

A silicon X-ray map (see Figure 7) reveals that Si is distributed fairly uniformly except in the 10-micron outer layer where the Si concentration is considerably less. Based on experimental work not discussed in this article, we believe the surface layer is due to a small fraction of the catalyst originally on the SiO_2 support that dissolves in the liquid monomers and catalyzes liquid-phase polymerization. This polymer precipitates from the liquid phase as very small, perhaps colloidal, particles, which are eventually deposited on the surface of the larger granules formed by the supported catalyst.

The composition of the copolymer along the granule radius was measured by FTIR microscope analysis for microtomed 250- and 750-micron particles produced at 5 and 20 min polymerization times. The FTIR beam was focused on a spot about 50×50 in size, and the methyl absorbance at 1,377 cm^{-1} normalized by the C-H band at 1,466 cm^{-1} was used to characterize the amount of propylene in the copolymer. We lack a calibration for determining absolute compositions from these absorbance measurements; however, the results in Figure 8

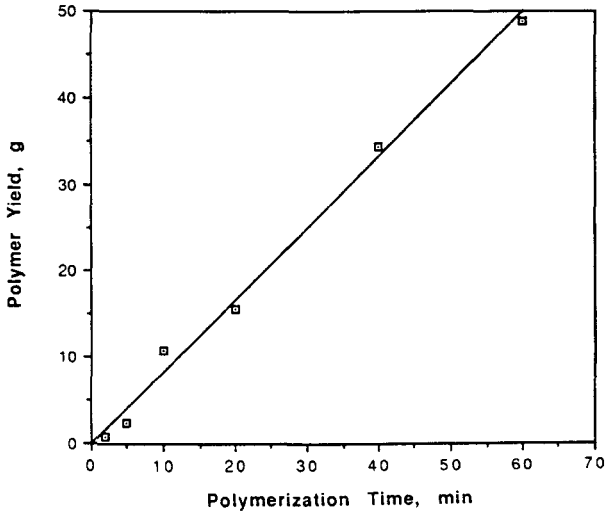

Figure 4. Dependence of yield on time in B catalyst polymerization.

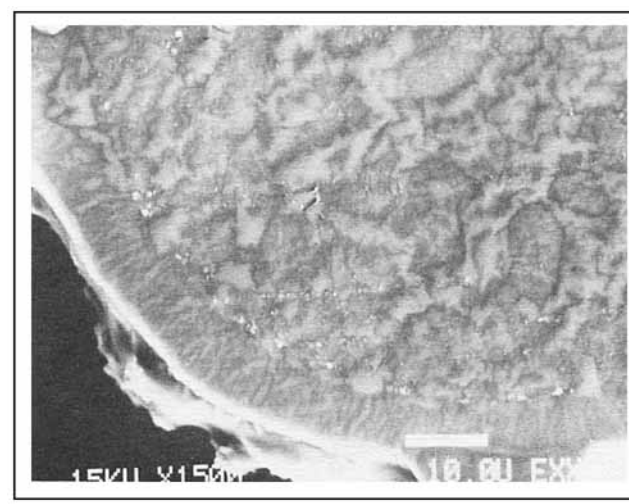

Figure 6. Granule morphology after 5-min polymerization.

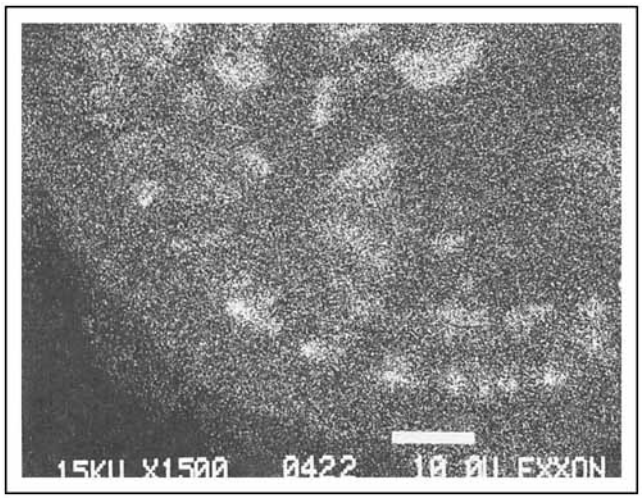

Figure 7. Si content map for the granule in Figure 6.

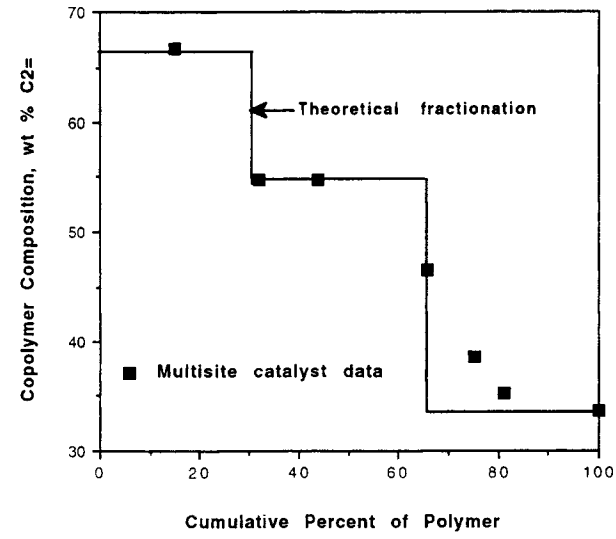

Figure 9. CD curve for polymer made with a multisited catalyst.

show that the propylene content of the copolymer is least at the surface of the granule and increases towards the center and that the change in composition from surface to center is greater for the large particle than for the small particle.

There are several possible causes for the broad composition distribution in copolymers made in slurry polymerization with supported metallocene catalysts. The most likely causes are multiple catalyst species, gas-liquid mass-transfer limitations in the laboratory reactor, and monomer diffusion effects within the growing polymer particle.

An advantage of plotting CD data as a cumulative weight percent is that it is easy to recognize CDs arising from multiple catalyst species. If a polymer consists of a blend of several compositions and a perfect fractionation is performed, the resultant CD curve should look like the solid line in Figure 9. For this hypothetical polymer, three compositions are present at 67, 55 and 33 wt. % ethylene representing 29, 36 and 35% of the total polymer. Also shown in this figure are the results of CD measurement for a polymer made with a multisited vanadium catalyst. It can be seen that the experimental CD data follows the theoretical curve for a polymer blend. However, the CD curve for the B catalyst polymer in Figure 1 is entirely different in shape and contains none of the inflections or plateau regions characteristic of polymers made by multisited catalysts. Furthermore, multisited catalysts tend to give products with broad MWD (although not always) and this was not observed with B catalyst polymers. The most significant argument against a multiple catalyst species explanation for broad CD is that it cannot account for the radial composition gradients shown in Figure 8 when the catalyst is distributed fairly uniformly throughout the growing particle.

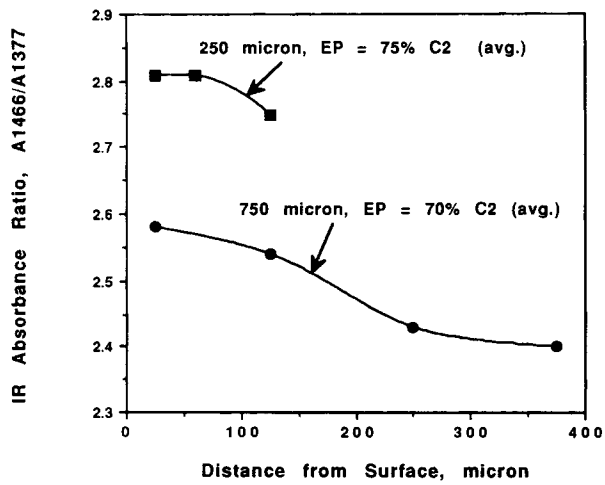

Figure 8. Copolymer composition gradient in granules made at 5- and 20-min reaction time.

At sufficiently high polymerization rates, the ethylene concentration in the laboratory reactor liquid phase could differ from the equilibrium value if gas-liquid mass-transfer rates are not high enough to maintain the ethylene concentration constant as fresh monomer is added to the gas phase. We did not directly measure monomer concentration during laboratory polymerizations; however, polymerizations with catalysts A and B were also run in a continuous flow pilot-plant reactor where the vapor-phase compositions were analyzed by GC. The GC results showed the gas and liquid phases to be in thermodynamic equilibrium and at constant composition over time, and the polymer made in the continuous flow reactor had the same CD breadth as polymers produced in the laboratory semibatch reactor. Thus, it is doubtful that gas-liquid mass transport limitations caused the broad CD measured for the laboratory polymers.

This leaves monomer diffusion in the granule as the last possibility to be considered. If polymerization at catalyst sites embedded in a polymer granule depletes monomer faster than it can be replaced by diffusion, monomer concentration will be higher at the surface of the granule, which is in contact with the fluid phase, than at the center. For homopolymerization, the existence of monomer concentration gradients will affect primarily polymerization rate, molecular weight, and MWD. In copolymerization with comonomers of unequal reactivity, monomer gradients will additionally cause the copoly-

mer composition to vary with both radial position and time. Thus, diffusion limitations could possibly explain the composition and CD results discussed earlier. In the following, we further explore whether diffusion effects provide a valid explanation of our experimental results by comparing the measured polymerization rate and CD data to the predictions of a mathematical model for diffusion controlled polymerization in a growing granule.

Modeling of Granule Growth

A number of models have been proposed for calculating the course of the polymerization as a function of time and particle radius. A polymerization model for polymer granule growth in which the active sites are dispersed throughout the particle was first proposed by Singh and Merrill (1971) and Schmeal and Street (1971). In this model, now often referred to as the polymeric flow model, the catalyst sites are considered to be molecularly dispersed in a continuum of polymer, and to move outward towards the surface as the spherical granule expands due to polymerization. The particle is considered to be nonporous, and a single diffusion coefficient characterizes the diffusion of monomer into the polymer. However, Schmeal and Street (1971) recognized that a polymeric macroparticle could consist of a large number of smaller microparticles and that either diffusion in the pores of macroparticle or in the microparticles could be rate limiting. Galvan and Tirrell (1986a,b) and Galvan (1986) extended the polymeric flow model to the case of copolymerization and to polymerization with two active sites.

Nagel et al. (1986) proposed the multigrain model for granule polymerization which views the granule as a macroparticle consisting of a large number of microparticles, each of which has an active site fixed in the center. The microparticles are assumed to be arranged in a series of concentric shells, and as the polymerization proceeds, the shells expand and the macroparticle grows. Two diffusion coefficients are required for this model, one for diffusion in the pores and one for diffusion in the microparticles. Ray and coworkers have examined this model in detail to predict the effect of diffusion on polymerization rate and polymer properties (Floyd et al., 1986, 1987; Hutchinson et al., 1992). Using parameter estimates thought to be characteristic for olefin homopolymerization with titanium chloride based catalysts, Floyd et al. (1986) showed that mass transfer in the granule pores is likely to be the limiting diffusive process. Also, assuming a single type of active site, MWD was moderately broadened due to diffusion. Q Values of 3-4 were predicted after 15 min of polymerization. Floyd et al. also found that diffusion effects are at a maximum extent early in the polymerization and become less important as the particle grows. This is because the increase in particle radius has a greater effect on reaction rate, which is decreasing as r^3 due to dilution of the catalyst with the polymer that has formed, than on diffusion resistance. Hutchinson et al. (1992) have extended the multigrain model to copolymerization.

Several varieties of the polymeric flow and multigrain models have also been considered. Sarkar and Gupta (1991, 1992) used a combination of the two models to reduce computational time. Skomorokhov et al. (1989) propose that a double grain model more closely resembles an actual polymer particle. In this model, the microparticles are assumed to consist of even smaller particles, so that pore diffusion also occurs in the microparticles and three diffusion coefficients are needed to describe the system. It should be noted that all of the models for polymer granule growth provide very simplified descriptions of the real phenomena. Although in some cases, morphology studies on crystalline polymers lend support to a multigrain model (Kakugo et al., 1989), other investigations have shown that polymerization can produce very complex granule structures (Wristers, 1973; Akar et al., 1983; Kim and Woo, 1989) that would not be well described by spherical microparticles assembled into a spherical macroparticle.

For essentially amorphous polymers it is doubtful that the particle porosity would be very high. Consequently, we selected the polymeric flow model as the best choice to represent granule growth during ethylene-propylene copolymerization. Thus, we consider the initial particle to be spherical with the active catalyst sites molecularly dispersed in the support matrix. As polymerization occurs, the catalyst becomes diluted with the polymer that is formed and flows outward as the particle radius increases.

The chain propagation reactions in copolymerization are:

$$\begin{aligned} P_i + M_1 &\Rightarrow P_{i+1} \quad k_{11} \\ P_i + M_2 &\Rightarrow Q_{i+1} \quad k_{12} \\ Q_i + M_1 &\Rightarrow P_{i+1} \quad k_{21} \\ Q_i + M_2 &\Rightarrow Q_{i+1} \quad k_{22} \end{aligned}$$

where

M_1, M_2 = monomer 1 and 2
P_i = growing chains i units long ending in M_1
Q_i = growing chains i units long ending in M_2
k = rate constant

Subscript 1 denotes ethylene and subscript 2 propylene. Since a prepolymerized catalyst was used in this study, chain initiation has already occurred before the catalyst is added to the reactor. Also, our data show a constant polymerization rate, at least up to the longest times studied (75 min), so catalyst deactivation is not significant. Finally, we will not attempt to model molecular weight or molecular weight distribution, so chain transfer reactions are not included in the model. Based on the calculations of Floyd et al. (1986), neither do we consider the possibility of particle temperature gradients.

This leads to the following reaction rate expressions for M_1, M_2, P and Q:

$$R_1 = -M_1(k_{11}P + k_{21}Q) \tag{1}$$

$$R_2 = -M_2(k_{22}Q + k_{12}P) \tag{2}$$

$$R_p = -k_{12}PM_2 + k_{21}QM_1 \tag{3}$$

$$R_q = -k_{21}QM_1 + k_{12}PM_2 \tag{4}$$

where P and Q represent the total concentrations of P and Q ended chains. The total growing chain concentration is given by:

$$C = P + Q \tag{5}$$

In the growing granule, the variations of M_1 and M_2 with radius and time is given by the material balance equations:

$$\partial M_1/\partial t = (D_1/r^2)\partial/\partial r[r^2\partial M_1/\partial r] - R_1 \quad (6)$$

$$\partial M_2/\partial t = (D_2/r^2)\partial/\partial r[r^2\partial M_2/\partial r] - R_2 \quad (7)$$

The total moles of catalyst remains constant in the granule, but the concentration change due to dilution with polymer is expressed by the equation:

$$\partial C/\partial t = -(1/r^2)\partial/\partial r(r^2uC) \quad (8)$$

where u is the velocity at which the radius is increasing. Similarly, the equations for P and Q are:

$$\partial P/\partial t = (-1/r^2)\partial/\partial r(r^2uP) - k_{12}PM_2 + k_{21}QM_1 \quad (9)$$

$$\partial Q/\partial t = (-1/r^2)\partial/\partial r(r^2uQ) + k_{12}PM_2 - k_{21}QM_1 \quad (10)$$

A relationship for the radial velocity, u, is obtained by equating the rate of volume increase to the volumetric reaction rate:

$$(1/r^2)\partial/\partial r(r^2u) = (1/\rho)(mw_1R_1 + mw_2R_2) \quad (11)$$

where mw_1 and mw_2 are the monomer molecular weights and ρ is the granule density.

The set of differential Eqs. 6-11 describing reaction/diffusion in a growing granule is a straightforward extension of the homopolymerization model of Schmeal and Street (1971) previously adapted to copolymerization by Galvan (1986). However, in comparison to previous work, we retain the accumulation terms $\partial M_1/\partial t$ and $\partial M_2/\partial t$ when solving the model equations and make no quasi-steady-state assumptions.

The boundary condition on the model are:

(1) Constant surface concentration of monomer:

$$M_1 = M_{10}$$
$$M_2 = M_{20}$$
$$\text{at } r = r_s$$

(2) Symmetric distribution of monomers at the center of the particle:

$$\partial M_1/\partial r = 0$$
$$\partial M_2/\partial r = 0$$
$$\text{at } r = 0$$

(3) No motion of the center of the particle:

$$u = 0$$
$$\text{at } r = 0$$

(4) No flux of catalyst or polymer across the particle outer surface:

$$\partial C/\partial r = \partial P/\partial r = \partial Q/\partial r = 0$$
$$\text{at } r = r_s$$

Boundary condition 1 arises from the assumption that the monomer at the surface of the granule is always in equilibrium with the monomer at constant concentration in the surrounding fluid phase. Previous work (Schmeal and Street, 1972; Galvan, 1986) has also applied the boundary condition:

$$\partial C/\partial r = 0$$

at the center of the particle. However, this boundary condition is not correct for two reasons. Setting $\partial C/\partial r = 0$ at both 0 and r_s overspecifies Eq. 8 which is first order in r. $\partial C/\partial r = 0$ is redundant in Eq. 8 at $r = 0$ in view of the condition that $u = 0$, so $\partial C/\partial r = 0$ at $r = r_s$ is the correct boundary condition. We did not investigate to what extent this change in boundary conditions from past work affects the solution of the model equations.

The initial conditions are:

(1) Monomer concentration in the particle is initially uniform at the surface concentration:

$$M_1 = M_{10}$$
$$M_2 = M_{20}$$

for all r at $t = 0$.

(2) Catalyst concentration in the particle is initially uniform:

$$C = C_o$$

for all r at $t = 0$.

(3) Initial particle radius is r_o.

Condition 1 assumes that the initial catalyst particles saturate with monomer very quickly, which is reasonable in view of their small size and high porosity. As a consequence of condition 1, the initial concentrations of P and Q are assumed to be given by:

$$P_o = C_o/(1 + k_{12}M_{20}/k_{21}M_{10}) \quad (12)$$

$$Q_o = C_o/(1 + k_{21}M_{10}/k_{12}M_{20}) \quad (13)$$

which are derived from the copolymerization steady-state assumption:

$$k_{12}P_oM_{20} = k_{21}Q_oM_{10}$$

The model equations were put in dimensionless form and coded for computer solution as described by Byrne (1992, 1993). The numerical method of lines (NMOL) was used to reduce the system of partial differential equations to a system of ordinary differential equations, which were then integrated by the ODE solver VODE. The output of the program gave the reactant concentrations, M_1, M_2, P, and Q, as a function of radius and time, and from these results instantaneous and average polymerization rates and copolymer compositions were simultaneously calculated. We were particularly interested in modeling copolymer composition distribution for comparison to experimental data. Calculation of instantaneous polymer compositions and polymerization rates allows calculation of the distribution of chain segments with differing composition which we term the "instantaneous CD." This is defined as the weight fraction of polymer produced with a given instantaneous composition. It is calculated by dividing the granule into 50 radial shells at each instant of time and computing the amount and composition of polymers made in each shell. These are then summed over the total polymerization time. However, because our kinetics do not account for chain transfer we do not know how these segments are arranged into chains. If chain lifetimes are long and M_1/M_2 at the active site varies during chain growth, then there will be a considerable distribution of composition along the length of the chain, but probably a relatively narrow CD between chains. On the other hand, even if M_1/M_2 varies considerably over the course of the polymerization, it can be relatively constant during growth if there is a low ratio of chain growth time to total polymerization time. In this case, there is little CD along the chain but a broad CD between chains. In the limit of zero lifetime, the CD between

chains is equal to the instantaneous CD calculated by the model. At typical polymerization conditions in this study, about 5×10^7 g of polymer were produced per mole of catalyst. Polymer M_n was usually measured to be 5×10^4–10×10^4 which indicates that 500 to 1,000 chains are produced at each active site. Thus, chain growth time is much less than total reaction time, and the instantaneous CD should be a reasonable approximation to the CD measured by fractionation. However, instantaneous CD for a polymer will, of course, be broader than the experimental CD since chain lifetimes are finite.

We also note that for homopolymerization, making the material balance equations dimensionless indicates that the dependence of dimensionless monomer concentration on dimensionless time is a function only of the Thiele modulus:

$$T = r_o (k_{11} C_o / D_1)^{1/2}$$

Thus, from a knowledge of T alone it is possible to estimate whether granule growth will be affected by mass transport limitations. In copolymerization, the monomer balances give rise to two modulii, one for each monomer:

$$T_1 = r_o (k_{11} C_o / D_1)^{1/2}$$

$$T_2 = r_o (k_{22} C_o / D_2)^{1/2}$$

and in addition, these modulii appear in the equations multiplied by terms which are functions of monomer concentration and the rate constants. Consequently, in this case it is more difficult to anticipate whether mass transport will be important based on knowledge only of the Theile modulii.

Estimation of Model Parameters

The physical property and kinetic constants that appear in the preceding model are shown below:

r_o

C_o

M_{10}, M_{20}

D_1, D_2

$k_{11}, k_{22}, k_{21}, k_{12}$

r_o and C_o are known from the conditions of catalyst preparation. An initial radius of 72×10^{-4} cm is typical of the catalysts we synthesized, and this value was used in the modeling calculations. C_o was determined by assuming that each mole of metallocene deposited on the support initiated a polymer chain since it is very difficult to measure the actual active catalyst concentration. If less than 100% of the catalyst is active the value of the rate constants determined from the model will be equal to $1/f$ times the true value, where f is the fraction of active catalyst.

The model equations are based on monomer concentrations in the polymer phase. Since only the fluid-phase monomer concentrations are known, an equilibrium relationship is needed to calculate M_{10} and M_{20} as a function of temperature, pressure, and gas-phase composition. A number of equations have been proposed for predicting phase equilibrium for polyolefin/hydrocarbon mixtures, most recently by Chen, Economou, and Radosz (1992) and High and Danner (1990). We chose to use the equilibrium equation developed by Schotte (1982) to estimate M_{10} and M_{20} as a function of reaction conditions since it has been confirmed experimentally (Heuer et al., 1989). Calculations with this equation of state (EOS) model require values of characteristic parameters P^*, T^*, and V^* for the pure solutes and polymer and Henry's constants for the polymer/solute pairs. We used the parameter values, shown in Table 2, published by Schotte for ethylene. P, V, T data for a 40 wt. % ethylene copolymer provided by Walsh (1991) were fit to the Schotte EOS to get the characteristic parameter values for the copolymer. Walsh et al. (1992) indicate that these parameters depend slightly on polymer composition. Heuer et al. (1989) give characteristic parameters for propylene based on a correlation of density data above T_c. Since P^*, T^*, and V^* are temperature-dependent to some degree, we recalculated these parameters from published density data at 0–70°C, which spans the range of polymerization temperatures used in this study, and obtained the values shown in Table 2.

Table 2. Parameters for the Schotte EOS Equation

	P^* atm	T^* K	V^* cm³/g	$A^{(1)}$ atm	$B^{(1)}$ K
Ethylene	4,054	2,034	1,2475	9.1108	−780.61
Propylene	3,936	2,705	1,1869	9.3460	−1,444.4
EP Copolymer	4,723	5,951	0.9914		

(1)Coefficients in the Henry's law coefficient equation: $\ln H = A + B/T$ (K).

A study by Iwai et al. (1985) indicates that Henry's constant, H_1, is very similar for a given solute in both polyethylene and polypropylene, while Newman and Prausnitz (1973) found that the Flory interaction parameter is almost the same for polyethylene and ethylene-propylene copolymers. From these results it appears that H_1 for ethylene-propylene copolymers is not strongly dependent on polymer composition over the 0 to 100% ethylene range. Consequently, we use the H_1 values of Heuer et al. for the ethylene/propylene/polyethylene system to also represent H_1 for ethylene-propylene copolymers (see values in Table 2).

The monomer solubilities in amorphous ethylene–propylene copolymer at 40°C and at equilibrium vapor pressure, as existed in our polymerization reactor, calculated from Schotte's equations are shown in Figure 10. It can be seen that the polymer sorbs considerable amounts of propylene and a much smaller amount of ethylene. Polymer granules removed from the reactor typically had weight losses of 25–35% upon drying which is in agreement with the concentration of monomers indicated in the figure. The relationship between the propylene concentration in the vapor and polymer phases is strongly nonlinear at these high monomer concentrations and does not follow Henry's law. We note that the equation of state predicts solubility for a totally amorphous polymer. For semicrystalline materials monomer concentrations will be less because the crystalline phase limits the ability of the amorphous phase to swell.

The equation of state also predicts the density for the polymer/monomer solution and these values were used in the model equations. The density obtained in this way is very similar to

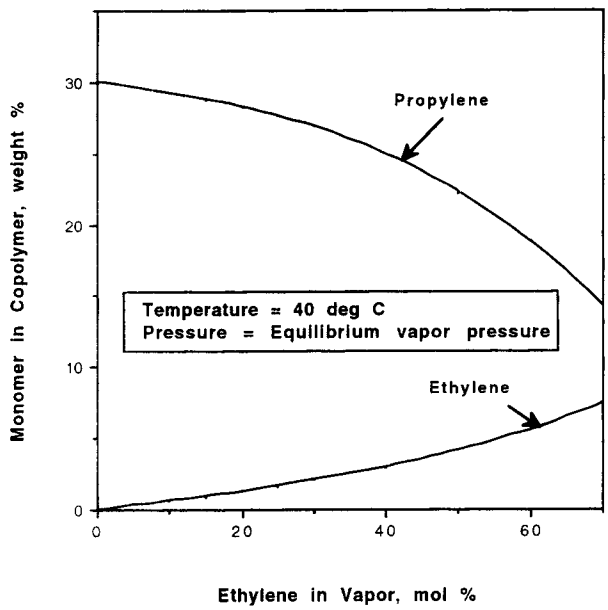

Figure 10. Calculated monomer solubility in EP copolymer.

a simple average density for the polymer and liquid propylene. A constant granule density was assumed in all calculations.

Unfortunately, the diffusion coefficients for ethylene and propylene in amorphous ethylene-propylene copolymers have not been measured. However, Michaels and Bixler (1961) provide values for these diffusivities in polyethylene and show that the diffusion takes place only in the amorphous phase. We assume that diffusion coefficients are similar in amorphous polyethylene and EP copolymer and use the equations presented by these authors to obtain the following estimates of D_1, and D_2, at 40°C and zero monomer concentration:

$$D_1 = 11.4 \times 10^{-7} \text{ cm}^2/\text{s}.$$
$$D_2 = 9.4 \times 10^{-7} \text{ cm}^2/\text{s}.$$

Kulkari and Stern (1983) measured the diffusivity of ethylene and propane in polyethylene and obtained values 30–50% lower than Michaels and Bixler. This was attributed to a difference in thermal history for the polyethylene which may have affected the fraction of amorphous phase. A recent review by Schlotter (1992) emphasizes the impact of crystallinity and morphology on diffusivity in polyethylene. It is well known that the diffusivity in amorphous polymer is a strong function of penetrant concentration in the polymer phase. In view of the high propylene concentration (see Figure 10) at reaction conditions, we expect that actual diffusion coefficients will be much higher than the values shown above. These values will be used only as initial estimates in the modeling calculations described later in this article.

Initial estimates of the propagation rate constants were obtained by neglecting mass transport effects and treating the polymerization data as if it were kinetically controlled. This will provide a lower bound on the rate constants. For polymerization with instantaneous initiation, no catalyst deactivation, and constant monomer concentration, polymerization rate is constant, and the rate Eqs. 1 to 4 yield the following expression for catalyst efficiency, G, in units of (moles of monomer reacted/mole of catalyst s):

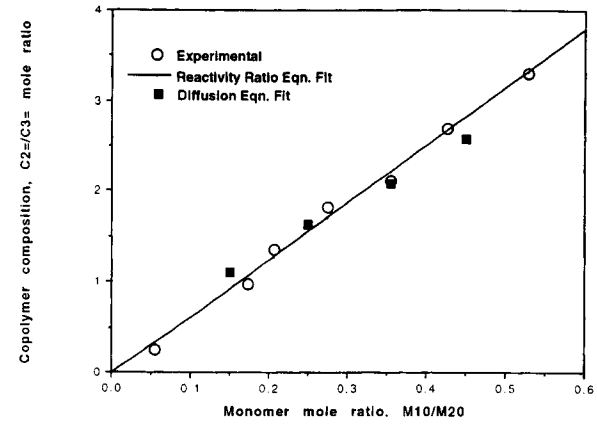

Figure 11. Dependence of composition of monomer ratio in A catalyst polymerization.

$$G = M_2[k_{22}/(1 + k_{22}F/k_{11})][(F + 1/r_2)M_1/M_2 + (1 + Fr_1)] \quad (15)$$

where
$F = r_1M_1/r_2M_2$
$r_1 = k_{11}/k_{12}$
$r_2 = k_{22}/k_{21}$
The copolymerization steady-state assumption:

$$k_{12}PM_2 = k_{21}QM_1$$

was made to obtain Eq. 15. This also leads to the copolymerization equation:

$$m_1/m_2 = (M_1/M_2)(r_1M_1/M_2 + 1)/(r_2 + M_1/M_2) \quad (17)$$

where m_1/m_2 is the comonomer mole ratio in the copolymer. If r_2 is equal to 0, Eq. 15 takes the form:

$$G = M_2[k_{21}/(1 + k_{21}M_1/k_{12}M_2)][(M_1/M_2)(r_1M_1/M_2 + 2)] \quad (18)$$

In the absence of chain termination, polymerization rates are constant and granule weight will increase linearly with time. Also, the monomer concentrations in Eqs. 15 to 18 will be given by M_{10} and M_{20}, the concentrations in equilibrium with the fluid phase.

For polymerization with A catalyst at 40°C, Eq. 17, the copolymerization equation, provides a good correlation for the dependence of copolymer composition ratio, m_1/m_2, on monomer ratio, M_{10}/M_{20}, as shown by the solid curve in Figure 11. The reactivity ratios giving the best fit to the data, as determined by nonlinear least-squares regression analysis, are:

$$r_1 = 6.5$$
$$r_2 = 0.17$$

With r_1 and r_2 known, k_{11} and k_{22} were determined from Eq. 15 by regression analysis of the relationship between G/M_{20} and M_{10}/M_{20}.

A plot of these two parameters (see Figure 12) at 40°C polymerization temperature supports a correlation between them, but there is a fair amount of scatter. A large part of

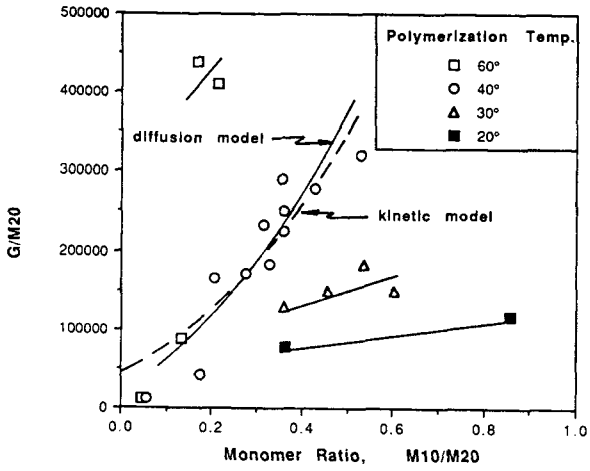

Figure 12. Dependence of polymerization rate on monomer ratio in A catalyst polymerization.

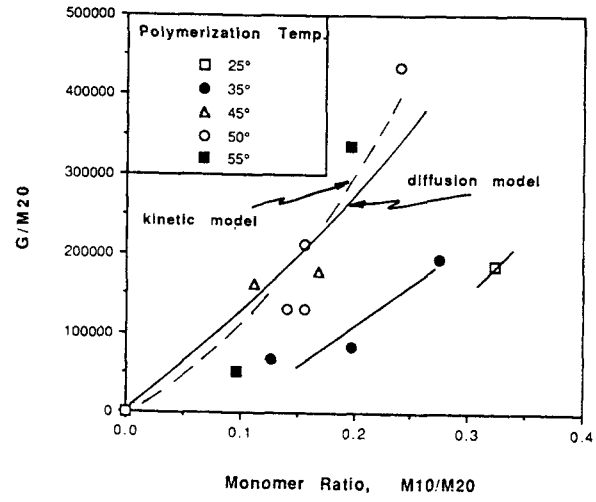

Figure 13. Dependence of polymerization rate on monomer ratio in B catalyst polymerization.

the scatter is caused by the difficulty of getting reproducible polymerization rates when small amounts of poison-sensitive coordination catalysts are used in batch reactions. However, the low G/M_{20} values at M_{10}/M_{20} ratios less than 0.20 are related to a loss of catalyst activity from the onset of severe particle agglomeration caused by the low polymer molecular weight characteristic of high propylene content copolymer. A least-squares regression of G/M_{20} vs. M_{10}/M_{20} gave:

$$k_{11} = 1.52 \times 10^6 \quad \text{cm}^3/\text{mol}\cdot\text{s}$$

$$k_{22} = 2.78 \times 10^4 \quad \text{cm}^3/\text{mol}\cdot\text{s}$$

and the correlation shown by the dashed curve in Figure 12. Dividing these rate constants by the reactivity ratios yields:

$$k_{12} = 2.36 \times 10^5 \quad \text{cm}^3/\text{mol}\cdot\text{s}$$

$$k_{21} = 1.64 \times 10^5 \quad \text{cm}^3/\text{mol}\cdot\text{s}$$

Data for A catalyst at other temperatures are also shown in Figure 12 to indicate the increase in G/M_{20} as temperature is raised. Not enough data is available at these other temperatures to quantify the effect of temperature on the polymerization rates.

A plot of G/M_{20} vs. M_{10}/M_{20} for polymerizations with B catalyst at 35 to 55°C is shown in Figure 13. Between 45 and 55°C there seems to be little effect of temperature on the relationship between these variables, although there is considerable scatter in the data. Polymerization at 35°C clearly results in a lower value of G/M_{20} at a given M_{10}/M_{20} ratio. It is apparent that polymerizations with B catalyst will be poorly described by Eqs. 15-18 since the change in polymer composition with time (see Figure 2) indicates the equations are inappropriate. Nevertheless, these equations are used to correlate the data so we can obtain initial estimates for the rate constants. For this estimation, the 45-55°C results were lumped into a single data set for analysis. The relationship between m_1/m_2 and M_{10}/M_{20} for these runs is shown in Figure 14. Fitting these data to the reactivity ratio equation indicates:

$$r_1 = 15.7$$

$$r_2 = 0$$

and gives the correlations shown by the solid curve in the figure. There is considerably more scatter from the correlation than in the case of A catalyst, which is not surprising in view of the dependence of polymer composition on reaction time and the range of temperatures represented by the data set.

Since $r_2 = 0$ (which is confirmed by the inability of B catalyst to homopolymerize propylene), Eq. 18 was used to estimate k_{21} and k_{21}/k_{12}. We found this equation poorly correlated the data in Figure 13 when r_1 was set to 15.7. So a second regression was carried out with r_1 left as a regression constant. This procedure gave:

$$k_{21} = 1.53 \times 10^5 \quad \text{cm}^3/\text{mol}\cdot\text{s}$$

$$r_1 = 42$$

but a specific value for k_{21}/k_{12} could not be determined because of insufficient variation in the range of M_{10}/M_{20} values. The

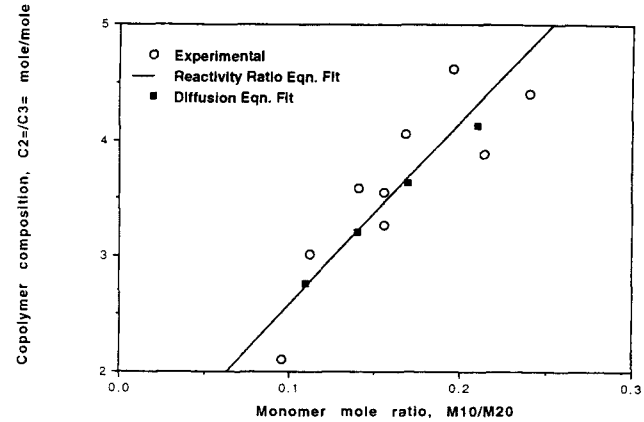

Figure 14. Dependence of composition on monomer ratio in B catalyst polymerization.

Table 3. Parameter Values Fit to the Diffusion/Reaction Model

	A Catalyst	B Catalyst
D_1, cm/s	1.68×10^{-5}	1.68×10^{-5}
D_2, cm/s	1.42×10^{-5}	1.42×10^{-5}
k_{11}, cm^3/mol·s	2.32×10^{6}	5.96×10^{7}
k_{12}, cm^3/mol·s	4.47×10^{5}	2.39×10^{6}
k_{22}, cm^3/mol·s	1.72×10^{4}	0
k_{21}, cm^3/mol·s	2.49×10^{5}	5.72×10^{5}

correlation only indicated that k_{21}/k_{12} was between 0 and 0.5. We arbitrarily chose $k_{21}/k_{12}=0.4$ for an initial estimate, which gives the set of initial B catalyst rate constants:

$$k_{11}=1.6\times10^{7}\quad \text{cm}^3/\text{mol}\cdot\text{s}$$

$$k_{21}=1.53\times10^{5}\quad \text{cm}^3/\text{mol}\cdot\text{s}$$

$$k_{12}=3.83\times10^{5}\quad \text{cm}^3/\text{mol}\cdot\text{s}$$

The difference in r_1 values as determined from Eqs. 17 and 18 with the same set of data is undoubtedly due to the broad composition distribution in the B catalyst polymer, which makes these equations inappropriate models.

Fitting of Data to Polymeric Flow Model

The technique used to fit data to the diffusion model is as follows. The rate constants and diffusion coefficients determined in the previous section represent minimum possible values. As mentioned earlier, monomer sorption into the polymer will increase diffusivities above the zero concentration values, and rate constants based on polymerization rates reduced by diffusion effects will, of course, be lower than the true rate constants. Indeed, making model calculations with the initial D and k estimates for A-catalyst gives polymerization rates much less than actually measured. We then increased D_1 and D_2 by a factor of 10 (to 11.4×10^{-6} and 9.4×10^{-6}), and raised rate constants until calculated and experimental catalyst efficiencies for the A catalyst data at 40°C were similar. However, the predicted CD breadth was broader than the measured CD breadth. D_1 and D_2 were increased further, with commensurate adjustments in k values to maintain a reasonably good prediction of polymerization rate, until predicted and measured CD breadth were in good agreement. Thus, there are a large number of combinations of D and k values that give the same predicted rates, and the CD data were used to choose the appropriate parameter values for the particular catalyst/copolymer system.

In view of the large number of estimated model parameters, the limitations in our data, and the assumptions in the model itself, it is not possible to determine D and k with a high degree of accuracy. However, the parameters given in Table 3 did a reasonable job of giving model calculations in good agreement with A catalyst experimental results. D_1 and D_2 in Table 3 are a factor of 15 higher than the values calculated earlier at zero monomer concentration. This is not an unreasonable increase in view of the high monomer solubility in the polymer (Fleischer, 1984). Rate constants are a factor of 2–5 higher than the initial estimates, and to get a correct prediction of polymer composition, reactivity ratios also had to be modified as shown below:

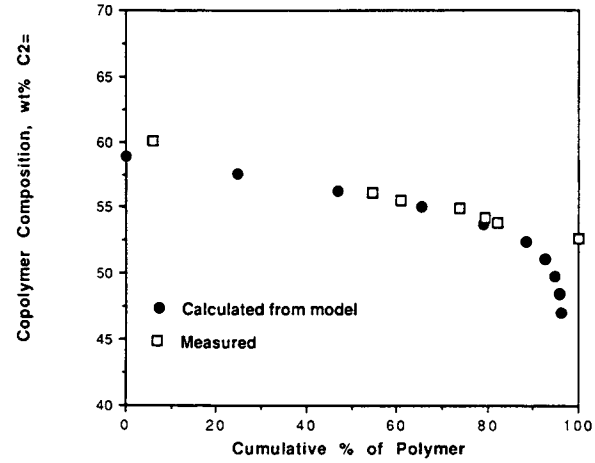

Figure 15. Comparison of calculated and measured CD for A catalyst polymerization.

	r_1	r_2
Initial (Kinetic Model)	6.5	0.17
Diffusion Model	5.2	0.069

Figure 15 shows the typical level of agreement between calculated and measured CD for A-catalyst polymers made at 40°C. The predicted CD matches the experimental data quite well, except for the presence of a tail of low ethylene content polymer in the calculated results. In our fractionation technique polymer of this nature would not be readily detected since it would all be lumped into the last fraction collected. Also, as mentioned earlier, the calculated and measured CDs are not defined in the same way, and it is not certain how well the calculated instantaneous CD should match the experimental values.

The dependence of catalyst efficiency (G/M_{20}) on M_{10}/M_{20} calculated from the diffusion model with the parameters in Table 3 is compared to the A catalyst experimental data in Figure 12. It can be seen that the kinetic model and diffusion model correlations do not markedly differ. A similar comparison is shown in the copolymer composition/monomer composition plots in Figure 11. The prediction of the diffusion model is essentially the same as from the reactivity ratio equation, Eq. 11. As shown in Figure 16, the diffusion model also

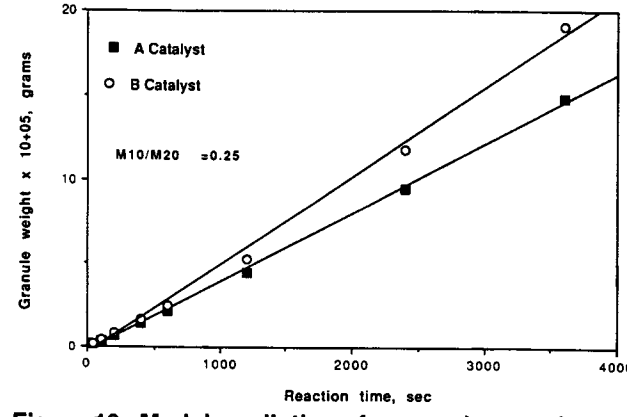

Figure 16. Model predictions for granule growth rate.

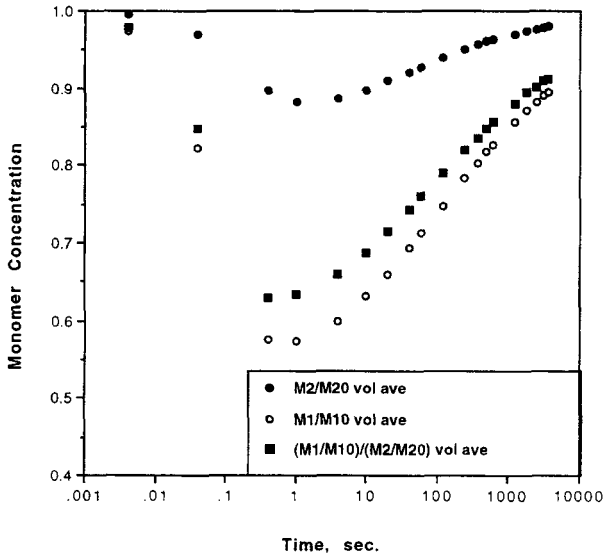

Figure 17. Calculated monomer gradients in A catalyst polymerization.

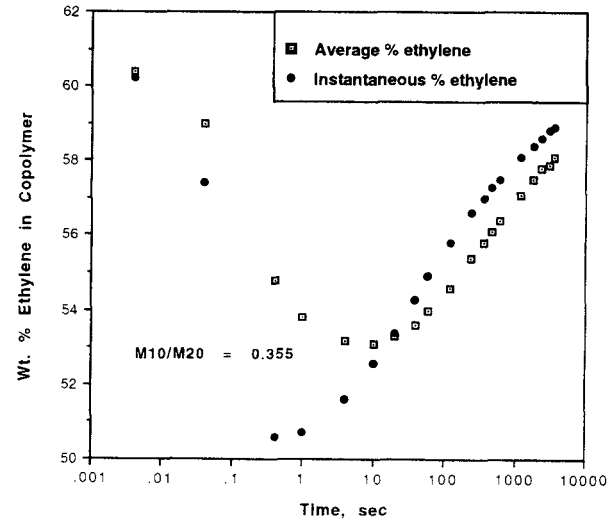

Figure 18. Calculated composition variations in A catalyst polymerizations.

predicts that with A-catalyst, at typical polymerization conditions, the increase in polymer weight with time, especially at times longer than 100 s, is approximately linear, again in accord with experimental observations. Thus, we conclude that the diffusion model does a good job of predicting the overall behavior of A-catalyst polymerization. The diffusion model and the kinetic model fit with appropriate parameter values give essentially similar predictions of polymerization rate even though the kinetic model, assuming homogeneous and time invariant monomer concentrations in the granule, is not correct. This fact points out the danger of concluding too much from overall rate data alone.

The extent of the diffusion effect on particle growth in A catalyst polymerization can be judged by the size of the monomer concentration gradients in the growing granule. To avoid the cumbersome presentation of monomer radial gradients as a function of time, we use the volume average monomer concentration in the granule:

$$M_v(t) = 1/V \int_0^{r_s} 2r^2 M(t)\,dt$$

where V is the granule volume corresponding to radius r_s, to characterize the overall monomer concentration at a given time. The ratio of M_v to the surface concentration indicates how much the average monomer concentration in the granule has been depressed by the effect of diffusion.

In a typical polymerization with A catalyst at $M_{10}/M_{20} = 0.355$, the calculated average ethylene concentration (see Figure 17) drops rapidly to 60% of the surface concentration in the first second of polymerization. The concentration then rises with further polymerization, reaching 80% of the surface concentration after 1 h (3,600 s). It may seem strange at first glance that diffusion effects diminish as the particle grows and its diameter increases. However, catalyst concentration is decreasing as the cube of the radius (due to dilution with polymer) slowing the rate of polymerization, and the surface area in contact with the bulk fluid is increasing with the square of the radius, raising the surface diffusion flux, while there is only a linear increase of the diffusion path length with radius. The net result is reduced diffusion influence in large particles. In comparison to the large variation in ethylene concentration, the concentration of the less reactive propylene remains relatively constant during particle growth. As a result, the variation of M_1/M_2 ratio with time, which controls polymer composition, closely tracks the variation of M_1.

Despite the fluctuation in M_1/M_2, the instantaneous average polymer composition (the volume average of the instantaneous compositions being produced at a given time) (see Figure 18) changes by only 6 wt. % between 10 s and 3,600 s polymerization time. The cumulative composition, which corresponds to the composition measured experimentally, changes by about the same amount during this period. The relative insensitivity of average composition to changes in the average M_1/M_2 ratio as the particle grows is primarily due to the values of the reactivity ratios for this catalyst. As shown by Eq. 17, changes in M_1/M_2 have the least effect on m_1/m_2 when the comonomer is readily incorporated.

To model the B catalyst data, all of the polymerization results at 45-55°C were considered as a single data set as was done in the earlier kinetic analysis. We then set the diffusion coefficient at the same value resulting from the A catalyst polymerization modeling, even though the temperature in these runs was 40°C, and again adjusted rate constants until the model gave a good prediction of overall reaction rate and polymer composition. With the rate constants in Table 3, catalyst efficiency and polymer composition calculated with the model match the data as well as the kinetic model correlation; however, there is still considerable scatter from the predicted values (see curves marked "diffusion model" in Figure 13 and Figure 14). r_1 for the diffusion model is 25 as compared to 42 for the kinetic model. As mentioned earlier in regard to the A-catalyst results, the calculated dependence of G/M_{20} on M_{10}/M_{20} and m_1/m_2 on M_{10}/M_{20} is remarkably similar for the kinetic and diffusion model. Particle growth is also predicted to be approximately linear with time (see Figure 16) at typical polymerization conditions.

However, as shown by the fractionation results for the B

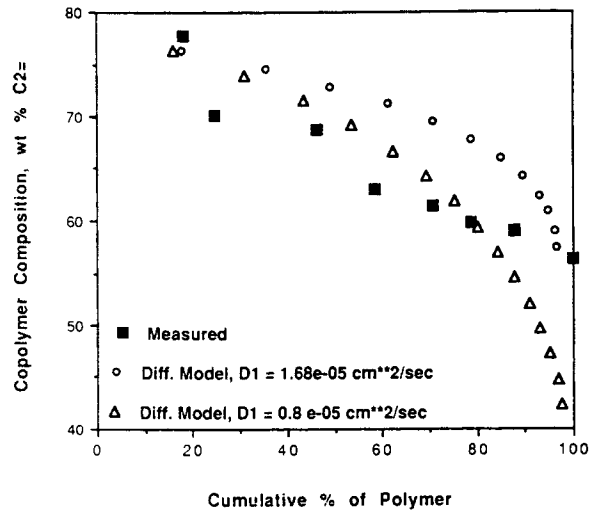

Figure 19. Comparison of calculated and measured CD for B catalyst polymerization.

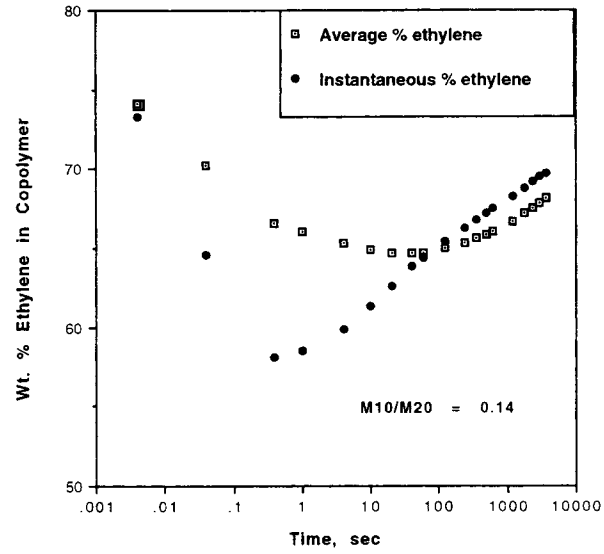

Figure 21. Calculated composition variations in B catalyst polymerization.

catalyst polymer in Figure 19, the calculated instantaneous CD only matches the end points of the measured CD, and the calculated distribution curve is convex as compared to a concave shape for the data. As a result, the percentage of polymer falling in a given composition range is quite different for the two CDs. To shift the calculated CD curve downwards towards the experimental data, the mass transport limitations in the model were increased by halving the diffusion coefficients and doubling the rate constants (to keep the overall polymerization rate about the same). This produces the second calculated curve in Figure 19, which still has the wrong shape and incorrectly predicts a large amount of polymer below 60 wt. % ethylene will be formed.

With the B catalyst parameters in Table 3 the model predicts a negligible change in propylene concentration in the particle with time, but ethylene concentration and M_1/M_2 ratio are much more severely affected by diffusion than in the case of A catalyst, as indicated in Figure 20. This causes a wide spread of instantaneous compositions, and a large drift of cumulative composition with time (see Figure 21). However, note that the model predicts the cumulative ethylene content rises between 2 min and 1 h polymerization time, while the experimental data show a decrease (see Figure 2). We were unable to find a set of parameter values that resulted in decreasing copolymer composition over a one-hour polymerization time. As mentioned above, the model always indicates that polymer ethylene content, after an initial drop, rises early in the polymerization due to decreasing mass transport effects as the particle grows.

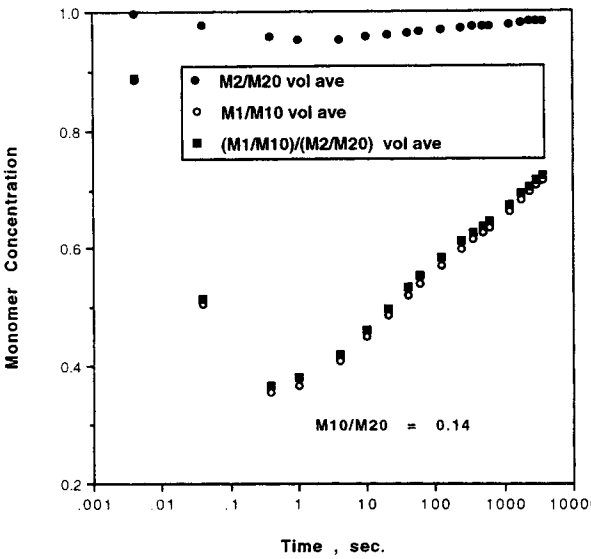

Figure 20. Calculated monomer gradients in B catalyst polymerization.

Although parametric studies with the model indicate that it is not capable of matching the CD and composition/time dependence observed in B catalyst polymerization, nevertheless we feel that diffusion effects are responsible for the characteristics of these polymers and that the model fails in this case because it assumes a constant diffusion coefficient. All of the copolymers made with B catalyst had compositions present that would be expected to be semicrystalline over the temperature range of the polymerizations. Because monomer solubility, and hence diffusivity, decrease with an increase in crystallinity, a composition gradient in the granule will result in a diffusivity gradient in these polymerizations. On the other hand, the A catalyst polymers were essentially amorphous and composition gradients do not affect diffusivity.

At this time, we cannot say how diffusivity and solubility gradients in a granule would be expected to influence polymerization behavior because the situation is obviously quite complex. However, if this is the correct explanation for the discrepancy between model predictions and B catalyst polymer measurements, then we can conclude that these gradients have a significant influence on the course of the polymerization.

As shown by the comparison of CD in Figure 22 for two B catalyst polymers of the same composition made at 35 and 50°C, CD narrows as temperature is raised. Since the polymerization rate increased at the higher temperature (see polymerization data in Table 1), this result may appear contra-

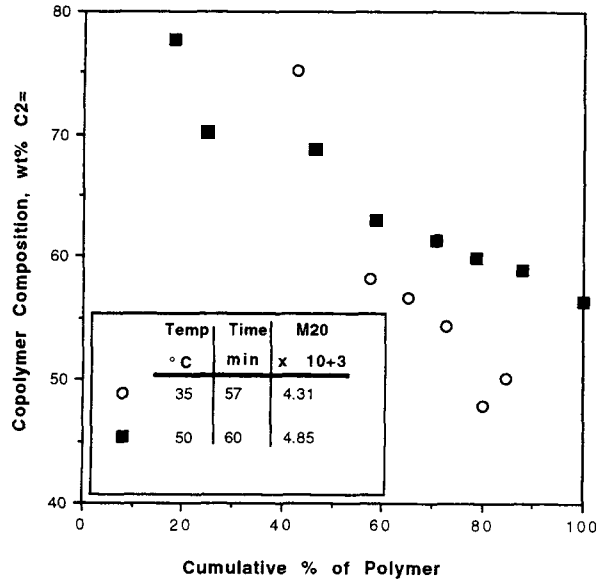

Figure 22. Effect of polymerization temperature on CD for B catalyst polymers.

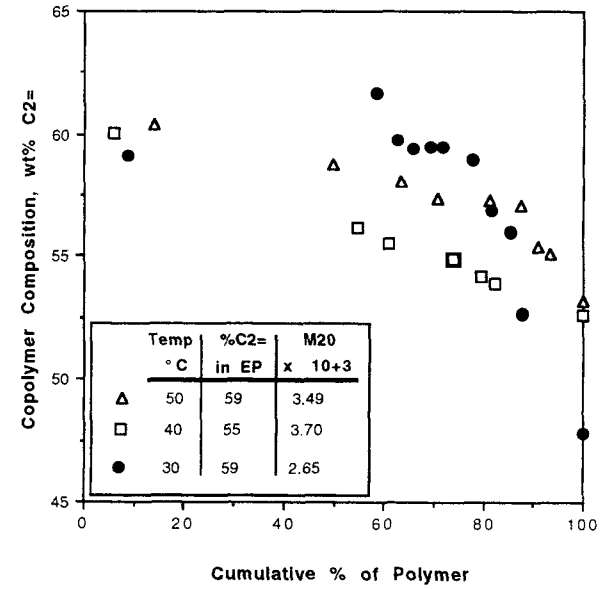

Figure 23. Effect of polymerization temperature on CD for A catalyst polymers.

dictory for a diffusion controlled polymerization. However, in our polymerization at monomer vapor-liquid equilibrium, there is an added effect of temperature on diffusivity due to its influence on monomer concentration. The term (k/D) appearing in the Thiele modulus can be written:

$$k/(D(0)\times g)$$

where $D(0)$ is the diffusivity at zero concentration and g is a factor to account for the increase in diffusivity with monomer concentration. Literature data (Kaminsky and Schlobolm, 1986; Chien and He, 1991) indicate that the chain propagation constants for copolymerization with metallocene catalysts have a temperature activation energy of about 10 kcal/mol, which is similar to the activation energy for $D(0)$ reported by Michaels and Bixler (1961). Thus, $k/D(0)$ will be relatively unchanged as temperature varies. On the other hand, the total monomer concentration in the polymer at equilibrium (see Table 2) at 35° is lower than at 50°C, which will reduce diffusivity. Also, for the semicrystalline polymer made with B catalyst, at 35°C the polymer is well below the melting point of 40–45°C, which further reduces the monomer concentration in the polymer phase. Variation in the parameter g caused by these solubility effects could explain the narrower CD at the higher temperature.

Similar results were also found with A catalyst. As shown in Figure 23, two polymers made at 40 and 50°C have similar CD breadths, although the CD of the 40°C polymer is shifted to lower ethylene contents because the average ethylene content is less. However, for the polymer made at 30°C, the CD is appreciably broader. These results can be correlated with the propylene solubility in the polymer during polymerization. The propylene concentration was about the same in the 40 and 50°C polymerizations (3.49 and 3.70 × 10-3 mol/cm^3, respectively, see Table 2) and much less at 30°C (2.65 × 10-3 mol/cm^3). Thus, we conclude that the observed effect of temperature on CD in this study is in accord with diffusion limitations during granule growth.

Discussion

In this article we present data showing that copolymers made with single-sited catalysts in slurry polymerization have an unexpectedly broad composition distribution. Based on the data analysis and modeling results in this study, we conclude that monomer mass transport limitations in the polymer particles during granule growth are the most probable explanation for the broad CD. This is the first experimental evidence we are aware of that diffusion can have a significant effect on copolymer properties in heterogeneous polyolefin polymerization. However, our results are limited to essentially amorphous granules with very low porosity. For copolymers of higher crystallinity, such as LLDPE, more porous polymer granules are produced, and diffusional effects may be quite different.

The data discussed in this article were obtained in a program that was not designed to measure diffusion effects. Consequently, some key experiments were not performed that would have provided additional evidence for a mass transport limitation explanation of our results. In particular, the modeling work indicates that initial catalyst particle radius has a strong influence on the extent of diffusion control. At the conditions of our polymerizations, the model predicts that with A catalyst, a threefold decrease in radius at constant catalyst concentration is sufficient to give considerable broadening of the CD. CD measurements for catalysts with different particle sizes could have greatly added to our understanding of the granule growth process.

Although we feel that mass transport limitations are the most likely cause of broad CD, a detailed explanation for the narrower CD in polymers of the same average ethylene content made with A catalyst instead of B catalyst is less certain. The major difference between these catalysts lies in the values of their reactivity ratios. Catalyst B has $r_2 = 0$ and tends to produce high ethylene content, semicrystalline polymers. We postulate that diffusion coefficient gradients in granules of semicrys-

talline polymers can lead to significant CD broadening, but additional work is needed to confirm this. In addition, differentiating the steady-state copolymerization equation, Eq. 17, to obtain $d(m_1/m_2)/d(M_1/M_2)$ and then exploring the effect of r_1 and r_2 on this derivative indicates that over most of the r_1-r_2 parameter space in which $r_1 > 1$ and $r_2 < 1$, the usual boundaries for olefin copolymerization with coordination catalysts, the amount of change in m_1/m_2 with a change in M_1/M_2 decreases as r_2/r_1 gets larger. Thus, in the presence of a given composition gradient, we would expect a broader CD to result with B catalyst than with A catalyst in view of the r_2/r_1 ratio differences.

For the D_1, D_2, k_{11} and k_{22} values determined from the modeling work, and with $r = 7.2 \times 10^{-3}$ cm and $C_o = 1 \times 10^{-5}$ mol/cc, the Thiele modulii for A and B-catalysts are:

	Thiele Modulus	
	Catalyst A	Catalyst B
Ethylene	84.6	429
Propylene	7.92	0

The modulii are larger for ethylene than for propylene, indicating that the ethylene polymerization rate is more readily affected by diffusion. But other than this, not much can be concluded from the modulii since the monomer polymerization rates depend on k_{12} and k_{21}, as well as k_{11} and k_{22}. Also, the modulii could be the same for two catalysts and yet the copolymer CD breadth could be different, depending on the value of the reactivity ratios. For example, with $C_o = 1.2 \times 10^{-5}$ and $M_{10}/M_{20} = 0.45$, the model predicts that after two hours of polymerization with A catalyst, copolymer is produced with an average ethylene content of 63.8 wt. % and 97% of the polymer is between 54.4 and 65.8 wt. % ethylene. If this calculation is repeated with k_{12} reduced by 1/2 so that r_1 is doubled but the Thiele modulii remain unchanged, the average ethylene content of the copolymer increases to 73.8%, and 97% of the polymer now lies between 62 and 76.6 wt. % ethylene. The broader CD in this case is due to the higher r_1 value.

As discussed earlier, the polymeric flow model with constant diffusivity is not adequate to model copolymerization when semicrystalline polymers are formed. We feel that none of the existing particle reaction/diffusion models appropriately describe granule growth in this situation. The multigrain model (Nagel et al., 1986) was initially developed to explore the effect of diffusion on the MWD of crystalline olefin homopolymers (polyethylene and polypropylene). For this case, modeling studies (Floyd et al., 1986) have shown that the major diffusion resistance is in the granule pores rather than in the polymer comprising the micrograins. Consider a series of copolymerizations in which increasing amounts of comonomer are incorporated in the polymer causing crystallinity to be reduced. At some point, the polymer becomes soft enough so that the micrograins begin to agglomerate. Thus micrograin diameter and particle porosity, both of which are parameters in the model, increase and decrease, respectively, as comonomer content increases. Eventually, diffusion through the micrograins rather than the pores becomes limiting, and at sufficiently high comonomer level, the porosity reaches zero and the multigrain model moves to the polymeric flow model.

In addition, if significant diffusion limitations occur, the radial copolymer composition gradients cause radial variations in crystallinity, which in turn result in radial gradients for diffusivity and monomer solubility. There could also be radial gradients in micrograin diameter and porosity resulting from the radial composition variation. This is an extremely complex physical situation that no model currently represents. Also, the lack of fundamental data or correlations relating diffusivity and monomer solubility to copolymer composition or crystallinity increases the already difficult challenge of modeling the granule growth process. Thus, it may not be practical to expect models to provide good predictions of diffusion controlled polymerization for semicrystalline polymers, except in a few special cases.

Notation

C = total catalyst concentration, mol/cm^3
D_1 = diffusion coefficient for monomer 1, cm^2/s
D_2 = diffusion coefficient for monomer 2, cm^2/s
G = catalyst efficiency, mol monomer/mol catalyst s
k = rate constant, cm^3/mol·s
m_1 = monomer 1 mol fraction in copolymer
m_2 = monomer 2 mol fraction in copolymer
M_1 = monomer 1 concentration, mol/cm^3
M_2 = monomer 2 concentration, mol/cm^3
M_v = volume average monomer concentration, mol/cm^3
P = concentration of M_1, ended growing chains, mol/cm^3
Q = concentration of M_2 ended growing chains, mol/cm^3
r = radial distance from particle center, cm
r_o = initial particle radius, cm
r_s = particle radius at time t, cm
r_1 = reactivity ratio, k_{11}/k_{12}
r_2 = reactivity ratio, k_{22}/k_{21}
t = time, s
T = Thiele modulus
u = rate of particle radial expansion, cm/s
ρ = particle density, g/cm^3

Subscripts

1 = monomer 1
2 = monomer 2
0 = initial condition

Literature Cited

Akar, A., N. C. Billingham, and P. D. Calvert, "The Morphology of Polyethylenes Produced by Alumina Supported Zirconium Tetrabenzyl," *Polymer*, **24**, 889 (1983).

Bul, V. W., and T. L. Higgins, "A Uniform Site Theory of Ziegler Catalysis," *J. Poly. Sci. Pt. A-1*, **8**, 1037 (1970).

Byrne, G. D., "The Solution of a Copolymerization Model with VODE," *Recent Developments in Numerical Methods and Software for ODEs/DAEs/PDEs*, G. D. Byrne and W. E Schiesser, eds., World Scientific, River Edge, NJ (1992).

Byrne, G. D., "The Taming of a Copolymerization Problem With VODE," *IMPACT of Computing on Science and Engineering*, **5**, 318 (1993).

Chen, S. J., I. G. Economou, and M. Radosz, "Density Tuned Polyolefin Phase Equilibria: 2. Mulicomponent Solutions of Alternating Poly (Ethylene-Propylene in Subcritical Olefins. Experiments and the SAFT Model," *Macromolec.*, **25**, 4987 (1992).

Chien, J. W., and D. He, "Olefin Copolymerization with Metallocene Catalysts I. Comparison of Catalysts," *J. Poly. Sci., Pt. A. Poly. Chem.*, **29**, 1585 (1991).

Cozewith, C., "Interpretation of 13C NMR Sequence Distribution for Ethylene-Propylene Copolymers Made with Heterogeneous Catalysts," *Macromolec.*, **20**, 1237 (1987).

Fleischer, G., "A Pulsed Field Gradient NMR Study of Diffusion in Semicrystalline Polymers," *Coll. and Poly. Sci.*, **262**, 919 (1984).
Floyd, S., K. Y. Choi, T. W. Taylor, and W. H. Ray, "Polymerization of Olefins through Heterogeneous Catalysis: III. Polymer Particle Modelling with an Analysis of Intraparticle Heat and Mass Transfer," *J. Appl. Poly. Sci.*, **32**, 2935 (1986).
Floyd, S., T. Heiskanen, T. W. Taylor, G. E. Mann, and W. H. Ray, "Polymerization of Olefins through Heterogeneous Catalysis. IV. Effect of Particle Heat and Mass Transfer on Polymerization Behavior and Polymer Properties," *J. Appl. Poly. Sci.*, **33**, 1021 (1987).
Galvan, R., "Modeling of Heterogeneous Ziegler-Natta Copolymerization of Olefins," PhD Thesis, Univ. of Minnesota (1986).
Galvin, R., and M. Tirrell, "Molecular Weight Distribution Predictions for Heterogeneous Ziegler-Natta Polymerization Using a Two-Site Model," *Chem. Eng. Sci.*, **41**, 2385 (1986a).
Galvan, R., and M. Tirrell, "Orthogonal Collocation Applied to Analysis of Heterogeneous Ziegler-Natta Polymerization," *Comp. and Chem. Eng.*, **10**, 77 (1986b).
Haejaski, T., Y. Inone, and R. Chujo, "Ethylene-Propylene Copolymerization Mechanism Based on the Sequence Distributions Determined by 13C NMR Spectra," *Macromolec.*, **21**, 3139 (1988).
Heuer, T., G. P. Peuschel, M. Ratzsch, and C. Wohlfarth, "Studies on the Solubility of Ethene, Propane, Propene, and 1-Butene in Molten Oligomers of Polyethylene and Ethene—Vinyl Acetate Copolymers: II," *Acta Polymerica*, **40**, 320 (1989).
Heuer, T., G. P. Peuschel, and C. Wohlfarth, "Studies on the Solubility of Ethene, Propane, Propene, and 1-Butene in Molten Oligimers of Polyethylene and Ethene—Vinyl Acetate Copolymers: I," *Acta Polymerica*, **40**, 272 (1989).
High, M. S., and R. P. Danner, "Application of the Group Contribution Lattice-Fluid EOS to Polymer Solutions," *AIChE J.*, **36**, 1625 (1990).
Hutchinson, R. A., C. M. Chen, and W. H. Ray, "Polymerization of Olefins through Heterogeneous Catalysis. X. Modeling of Particle Growth and Morphology," *J. Appl. Poly Sci.*, **44**, 1389 (1992).
Iwai, Y., M. Ohzono, and Y. Arai, "Gas Chromatographic Determination and Correlation of Weight-Fraction Henry's Constants for Hydrocarbon Gases and Vapors in Molten Polymers," *Chem. Eng. Commun.*, **34**, 225 (1985).
Kakugo, M., H. Sadatoski, J. Saki, and M. Yokoyama, "Growth of Propylene Particles in Heterogeneous Ziegler-Natta Polymerization," *Macromolec.*, **22**, 3172 (1989).
Kaminsky, W., and M. Schlobohm, "Elastomers by Atactic Linkage of Alpha Olefins Using Soluble Ziegler Catalysts," *Macromolec. Chem., Macromol. Symp.*, **4**, 103 (1986).
Kim, I., and S. D. Woo, "Morphological Study of HDPE Prepared with the highly Active Silica Supported $TiCl_4/MgCl_2$ Catalyst," *Poly J.*, **21**, 697 (1989).
Kulkarni, S. S., and S. A. Stern, "The Diffusion of CO2, CH4, C2H4, and C3H8 in Polyethylene at Elevated Pressure," *J. Poly. Sci., Poly. Phys.*, **21**, 441 (1983).
Michaels, A. S., and H. J. Bixler, "Flow of Gases through Polyethylene," *J. Poly. Sci.*, **50**, 413 (1961).
Nagel, E. J., V. A. Krillov, and W. H. Ray, "Predictions of Molecular Weight Distributions for High Density Polyolefins," *Ind. Eng. Chem. Prod. Res. Dev.*, **19**, 372 (1986).
Newman, R., and J. M. Prausnitz, "Thermodynamics of Concentrated Polymer Solutions Containing Polyethylene, Polyisobutylene, and Copolymers of Ethylene with Vinyl Acetate and Propylene," *AIChE J.*, **19**, 704 (1973).
Sarkar, P., and S. K. Gupta, "Simulation of Propylene Polymerization: An Efficient Algorithm," *Polymer*, **33**, 1477 (1992).
Sarkar, P., and S. K. Gupta, "Modelling of Propylene Polymerization in an Isothermal Slurry Reactor," *Polymer*, **32**, 2842 (1991).
Schlotter, N. E., and P. Y. Furlan, "A Review of Small Molecule Diffusion in Polyethylene," *Polymer*, **33**, 3323 (1992).
Schmeal, W. R., and J. R. Street, "Polymerization in Expanding Catalyst Particles," *AIChE J.*, **17**, 1188 (1971).
Schotte, W., "Vapor Liquid Equilibrium Calculations for Polymer Solutions," *Ind. Eng. Chem. Process Des. Dev.*, **21**, 89 (1982).
Singh, D., and R. R. Merrill, "Molecular Weight Distribution of Polyethylene Produced by Ziegler-Natta Catalysts," *Macromolec.*, **4**, 599 (1971).
Sinn, H., W. Kaminsky, H. J. Vollmer, and R. Woldt, "Living Polymerization on Polymerization with Extremely Productive Ziegler Catalysts," *Angew. Chem. Inter. Ed. Eng.*, **19**, 390 (1980).
Skomorokhov, V. B., V. A. Zakharov, V. A. Kirillov, and G. D. Bukatov, "Mass Transfer in Polymerization of Olefins on Solid Catalysts. The Double Grain Model," *Poly. Sci. U.S.S.R.*, **31**, 1420 (1989).
Stockmeyer, W. H., "Distribution of Chain Lengths and Compositions in Copolymers," *J. Chem. Phys.*, **13**, 199 (1945).
Walsh, D. J., W. W. Graessley, S. Datta, D. J. Lohse, and L. J. Fetters, "Equations of State and Predictions of Miscibility for Hydrocarbon Polymers," *Macromolec.*, **25**, 5236 (1992).
Walsh, D. J., personal communication (1991)
Wristers, J., "Nascent Polypropylene Morphology: Polymer Fiber," *J. Poly. Sci. Poly. Phys.*, **11**, 1601 (1973).
Yechevskaya, L. G., G. D. Bukatov, V. A. Zakharov, and A. V. Nosov, "Study of the Molecular Structure of Ethylene-Propylene Copolymers Obtained with Catalysts of Different Composition," *Macromol. Chem.*, **188**, 2573 (1987).
Zucchini, U., and G. Cecchin, "Control of Molecular Weight Distribution in Polyolefins Synthesized with Ziegler-Natta Catalyst Systems," *Adv. Poly. Sci.*, **51**, 101 (1983).

Manuscript received July 12, 1993, and revision received Oct. 22, 1993.